Korean J. Chem. Eng., 40(1), 104-111 (2023)
DOI: 10.1007/s11814-022-1287-9

pISSN: 0256-1115
eISSN: 1975-7220

Improved the hydrogen sorption properties of MgH_2 by CeMnZr solid solution

Ying Cheng*,, Wei Zhang***,†, Biqing Shi*, Siqi Li*, Bing Dong*, Yulian Quan*, and Xianbin Ji***

*Department of Environmental Engineering, Hebei University of Environmental Engineering, Qinhuangdao, 066102, P. R. China
**Hebei Key Laboratory of Agroecological Safety, Hebei University of Environmental Engineering, Qinhuangdao, 066102, China
***Hebei Key Laboratory of Applied Chemistry, School of Environmental and Chemical Engineering, Yanshan University, Qinhuangdao, 066004, P. R. China
(*Received 12 May 2022 • Revised 17 August 2022 • Accepted 13 September 2022*)

Abstract−Magnesium hydride (MgH_2) is one of the promising solid-state hydrogen storage materials because of its high capacity, abundant resource and excellent reversibility. However, the high dehydrogenation temperatures and sluggish kinetics restrict its practical application. It was found that doping catalysts could significantly improve the hydrogen storage properties of MgH_2. The solid solution $Ce_{0.8}Mn_{0.1}Zr_{0.1}O_2$ (denoted as CeMnZr) with abundant oxygen vacancy was synthesized and its catalytic influence on the hydrogen sorption properties of MgH_2 have been investigated. CeMnZr modified MgH_2 composite showed a reduced initial decomposition temperature, almost 62 K lower than the pristine MgH_2. At 473 K, MgH_2-CeMnZr composite had an absorption capacity of 4.08 wt% hydrogen within 3,500 s, which was about twice better than the pure MgH_2 at same condition. MgH_2-CeMnZr sample could desorb 2.56 wt% of H_2 within 3,500 s at 573 K compared to low desorption rate and 0.85 wt% H_2 by as-milled MgH_2. The activation energy (Ea) for CeMnZr codoped MgH_2 sample is about 50 $kJ \cdot mol^{-1}$ lower than the milled MgH_2. Based on the characteration analysis, the *in-situ* generated MgO and $CeH_{2.51}$ species as well as abundant oxygen vacancy is believed to play synergistic catalytic effects in enhancing the hydrogen storage properties of MgH_2.

Keywords: Magnesium Hydride, Composite, Solid Soultion, Hydrogen Sorption Performance, Hydrogen Kinetics

INTRODUCTION

The excessive consumption of fossil fuel leading to the seriously environmental crisis forces human beings to look for a new energy to supersede the traditional conventional energy fuels [1-4]. Hydrogen as a renewable energy possesses high hydrogen density, is pollution-free and non-toxic, making it become the competent candidate for the future energy system instead of fossil fuel [5-8]. Actually, the widespread utilization of hydrogen is limited by the concerns on safety and efficient storage. The conventional gaseous and liquid hydrogen storage method requires extremely harsh high pressure and low temperature, which easily causes serious equipment and security problems [9,10]. Solid-state hydrogen storage material has been considered as a suitable and benign alternative in hydrogen storage owing to its high capacity and safety. Among all the solid-state materials, magnesium-based hydrogen storage material, especially magnesium hydride (MgH_2), is one of the most prominent hydrogen storage materials due to its high capacity, large reserves and excellent reversibility [11-14]. For all its benefits, the widespread application of MgH_2 is still hampered: one is the relatively high dissociation temperature of MgH_2 over 400 °C, the other is the sluggish hydrogen absorption/desorption kinetics performance even at 300 °C [15-17].

Extensive researches have been focused on the improvement of the thermodynamic and dynamics behavior of MgH_2 by ball-milling, nano-structuring, alloying and doping catalyst, etc. However, it is confirmed that doping catalyst by transition metal is an efficient approach that can be used to accelerate the hydrogen storage performance of MgH_2. The rare earth Ce based catalyst exhibits remarkable hydrogen uptake/release properties for MgH_2. Zhang et al. introduced CeO_2 (20%) into pure MgH_2 [18]; their results proved that the uniformly distributed cerium oxides acting as the real catalysts helped the recombination of hydrogen and nucleation of new phase, which effectively promoted the hydrogen absorption/desorption behavior of MgH_2. In addition, nano CeO_2 with a particle size 10-15 nm was synthesized through ball-milling method and its catalytic role in the thermodynamic properties of MgH_2 was also investigated by Singh et al. [19]. They found the addition of 2 wt% CeO_2 into MgH_2 led to striking hydrogen absorption performance and relatively lower decomposition temperature. The added composite showed a 1.5 times absorption kinetics than the pristine MgH_2 and with a lower desorption temperature about 383 °C. CeO_2 modified Fe_2O_3 also presented excellent hydrogen storage properties as reported by Wang et al. [20].

Furthermore, abundant oxygen vacancies also played a vital role in the improvement of hydrogen properties of Mg-based compounds. Numerous works have proved that the excellent catalytic activity for CeO_2 on the Mg-based compounds is attributed to abundant oxygen vacancies, which helps to provide the defects of crystal boundary and further shortens the diffusion of hydrogen [21,

†To whom correspondence should be addressed.
E-mail: zhangweihh@ysu.edu.cn

22]. Xiong et al. found that the amount of oxygen vacancy on the Zr doped CeO_2 is much higher than the pure CeO_2 [23,24]. The transition meal modified CeZr sample exhibits the most oxygen vacancy than the CeZr compounds [25,26]. Mn also has a positive catalytic effect on the enhancement of hydrogen storage material [27]. Ismail et al. reported that the $MnFeO_4$ catalyst synthesized through hydrothermal method reduced the onset temperature and enhanced the hydrogen sorption kinetics; the remarkably improved hydrogen sorption was attributed to the in-situ formed Fe particle and Mn-containing phases [28]. And the synergistic catalytic effects of nanosized $Zr_{0.7}Ti_{0.3}Mn_2$ and MWCNT were also confirmed by Li et al. [29].

Inspired by the above, a Mn and Zr doped CeO_2 (donated as CeMnZr) solid solution catalyst with abundant oxygen vacancy was synthesized, and its catalytic effect on the hydrogen sorption properties on pure MgH_2 was systematically investigated. Moreover, the corresponding catalytic mechanism of the doped CeMnZr solid solution catalyst in hydrogen absorption/desorption process of MgH_2 is presented, which will give a better understanding for the diversified hydrogen storage catalyst.

EXPERIMENTAL

1. Synthesis of CeMnZr Solid Solution

$Ce(NO_3)_3{\cdot}6H_2O$ (99.9%), $Mn(NO_3)_2$ (50 wt%), $ZrOCl_2$ (99.9%) were purchased from Aladdin and directly used as reactant no further purification. The raw material with a molar ratio 8 : 1 : 1 (Ce : Mn : Zr=8 : 1 : 1) was dissolved into the mixture of solvent (ethylene glycol and deionized water) containing 0.1 mol ascorbic acid. After the mixed solution was stirred into a transparent solution, $NH_3{\cdot}H_2O$ was added into the above solution to keep the pH=10. The mixture was kept stirring 2 hours and then aged for 12 hours at room temperature. After aging, the precipitates were filtered and washed several times with deionized water, and dried at 60 °C for 12 h. Subsequently, the sample was calcined from room temperature to the target temperature of 500 °C with the heating rate of 2 °C/min. After holding at the target temperature for a period, the solid solution of $Ce_{0.8}Mn_{0.1}Zr_{0.1}O_2$ (denoted as CeMnZr) sample was obtained.

2. Synthesis of MgH_2-CeMnZr Composites

MgH_2 was prepared through the method of hydrogen combustion from the commercial Mg powder (98%). The Mg powder was hydrogenated at 400 °C for 10 h under the pressure of 4.0 MPa and the pure MgH_2 was successfully obtained by repeating the above procedure five times.

The doped MgH_2-CeMnZr sample was obtained by mechanically ball-milling MgH_2 with CeMnZr additive with the mass ratio of 5 : 1 under planetary grinding machine. The mixture was put into the stainless-steel milling vial with the ball-to-sample weight ratio 40 : 1. To avoid increased milling temperature, after each 30 min of ball milling, the milling vial was rested 15 min, and then launched in another different direction for 30 min. All the operation was undertaken in an Ar-filled glove box to prevent the oxidation and humidity.

3. Characterization

X-ray diffraction (XRD) was conducted by SmartLab high resolution X-ray diffractometer (made by Rigaku company) with the scanning range from 10° to 80° equipped with Cu Kα radiation at 40 kV, 40 mA. The microstructure and morphology of the samples were observed by scanning electron microscopy (SEM). X-ray photoelectron spectroscopy (XPS) was used to detect the surface element distribution and the active oxygen species of the composites doped and undoped. Raman was employed to further identify the composition of the sample, which was collected in the anti-Stokes range of 100-2,000 cm^{-1} using an inVia ReflexRenishaw spectrometer. The samples were excited using a He-Gd laser (excitation wavelength of 532 nm).

Temperature programmed desorption (TPD) and hydrogen sorption kinetics were investigated using Sieverts-type pressure-composition-temperature (PCT) apparatus (made by GRINM Co., China). TPD test with the heating rate of 10 K/min was carried out to determine the desorption properties of MgH_2 from room temperature to 873 K at 0.001 MPa under the vacuum chamber. During the hydrogen absorption kinetics test, the sample was heated at 423 K and 473 K under 3.0 MPa H_2, whereas for the hydrogen desorption kinetics test, the sample was heated at 573 K and 623 K under the pressure of 0.001 MPa. The thermal behavior of the as-milled MgH_2 and MgH_2-CeMnZr sample was detected by differential scanning calorimetry (Mettler Toledo TGA/DSC 1). All the samples were heated under Ar atmosphere from room temperature to 550 °C under various heating rates: 5 K/min, 10 K/min, 15 K/min, 20 K/min.

RESULTS AND DISCUSSION

1. Characterization of the Prepared CeMnZr

The phase constitution of the as-synthesized CeMnZr catalyst was detected by XRD analysis, and the XRD pattern of the synthesized CeMnZr is shown in Fig. 1. It is obvious that the sample exhibits sharp diffraction peaks, indicating the synthesized sample has a good crystal structure. Moreover, the dominant charactered peaks assigned to 28.86° (111), 33.52° (200), 47.48° (220), 56.34° (311), 59.09° (222), 69.42° (400), 76.70° (331), 79.08° (420) well match the standard card CeO_2 (PDF#34-0394). In Fig. 1(b), a strong adsorption peaks observed at approximately 460 cm^{-1} could be assigned to the Ce-O stretching vibrations in the samples, and there are no obvious Raman lines due to Mn-O or Zr-O are observed for CeMnZr catalyst, which implies that the doped metal ions integrated into the CeO_2 lattice framework forming a stable solid solution.

Additionally, the peaks from XRD and Raman analysis for the doped CeO_2 are much weaker and broader than that of pure CeO_2, which indicates the presence of more defective lattice and smaller crystallite size. Interestingly, the XRD peaks of the doped CeO_2 are shifted obviously to the right with a higher Bragg angle (Fig. 1(a)), caused by lattice shrinkage due to substitution of Ce^{4+} (0.097 nm) by transition metal ions with smaller ionic radii (Zr^{4+}=0.084 nm, Mn^{2+}=0.083 nm, Mn^{3+}=0.065 nm, and Mn^{4+}=0.053 nm) [30,31]. Meanwhile, the same characteristic peak shift could be seen from the Raman spectra as compared to the pure CeO_2, indicating the successfully synthesized solid solution CeMnZr catalyst.

2. Hydrogen Sorption Kinetics

The addition of CeMnZr exhibited excellent catalytic effects on

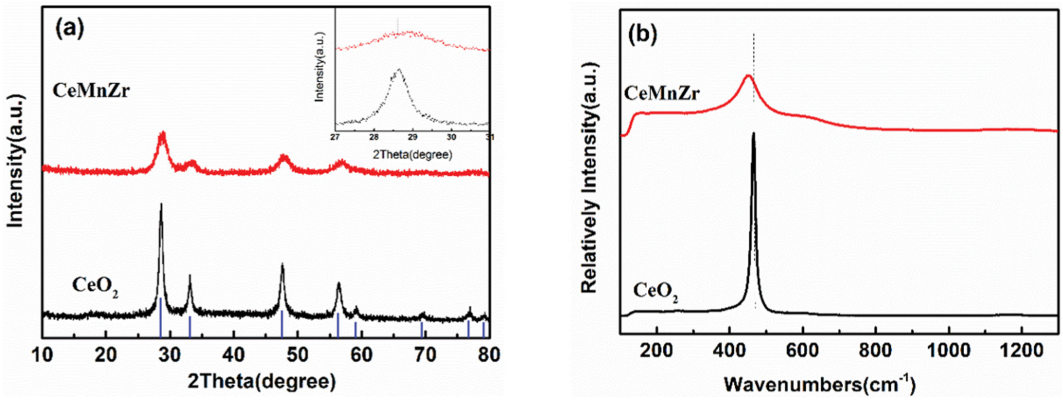

Fig. 1. (a) XRD pattern of the as-synthesized CeMnZr catalysts; (b) Raman spectra of the as-synthesized CeMnZr catalysts.

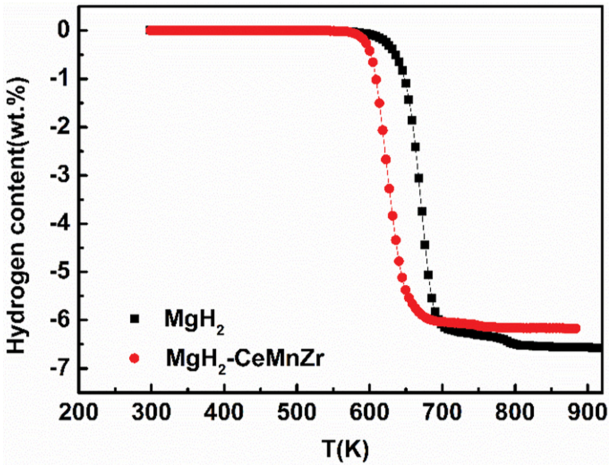

Fig. 2. The onset decomposition temperature curves for the as-milled MgH_2 and MgH_2-CeMnZr composite.

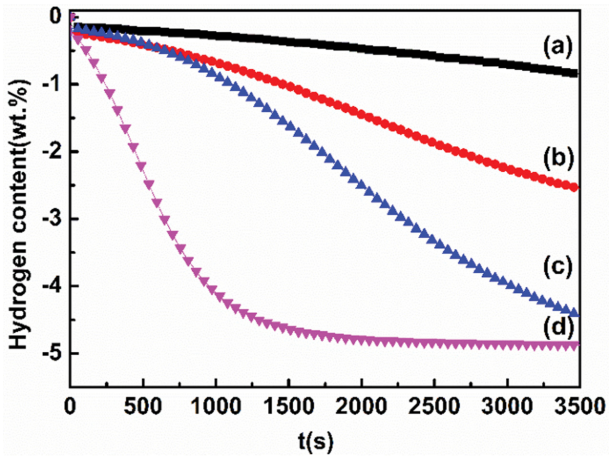

Fig. 3. Isothermal dehydrogenation curves of the samples: (a) MgH_2 at 573 K; (b) MgH_2-CeMnZr at 573 K; (c) MgH_2 at 623 K; (d) MgH_2-CeMnZr at 623 K.

the improvement of hydrogen storage properties of MgH_2, and the desorption curves of the hydrogen weight loss versus temperature characterization for the pristine MgH_2 and CeMnZr doped MgH_2 sample are presented in Fig. 2. The dehydrogenation of as-milled MgH_2 started at 643 K, with the maximum 6.5 wt% of hydrogen capacity released in the temperature range. The doped CeMnZr catalyst had a notable effect on the hydrogen decomposition temperature of MgH_2 and adding CeMnZr clearly reduced the initial decomposition temperature of MgH_2. The onset decomposition temperature for CeMnZr doped MgH_2 sample was 581 K, which was decreased by 62 K compared to as-milled MgH_2. The little decrease in the maximum hydrogen release for MgH_2-CeMnZr sample (6.2 wt%) is because the additive does not have the ability of hydrogen absorption/desorption. Obviously, CeMnZr is a positive catalyst that presented a brilliant result in reducing the initial desorption temperature of MgH_2.

The dehydrogenation properties of the as-milled MgH_2 and CeMnZr doped MgH_2 composite was further investigated by the isothermal reaction at 573 K and 623 K under 0.001 MPa. As seen from Fig. 3, almost no hydrogen could be desorbed by the pristine MgH_2 within 1,000 s at 573 K, and only 0.85 wt% hydrogen was detected in 3,500 s at the same temperature. Increasing the temperature significantly improved the desorption properties of MgH_2. When the temperature rises to 623 K, the hydrogen desorption ability is increased to 4.43 wt% within 3,500 s at 623 K, but the hydrogen desorption rate is still not satisfied. However, the hydrogen release property for the doped sample yields a striking improvement. The CeMnZr added sample liberates 2.56 wt% of hydrogen within 3,500 s at 573 K, which is more than twice than the as-milled MgH_2. Furthermore, the hydrogen desorption capacity and hydrogen release rate for the MgH_2-CeMnZr composite are obviously prior to the pristine MgH_2 and almost 4.87 wt% hydrogen is obtained at 623 K. From these data, it is concluded that CeMnZr solid solution exhibits excellent catalytic effect in boosting the hydrogen desorption kinetics of MgH_2.

The apparent activation energy (Ea) is a vital parameter which reflects how hydrogen desorption could happen. The improved hydrogen desorption ability is correlated to the energy barrier for the hydrogen released from MgH_2. The apparent activation energy (E_a) for the as-milled MgH_2 and CeMnZr doped sample is calculated by the Kissinger method; the corresponding equation is as

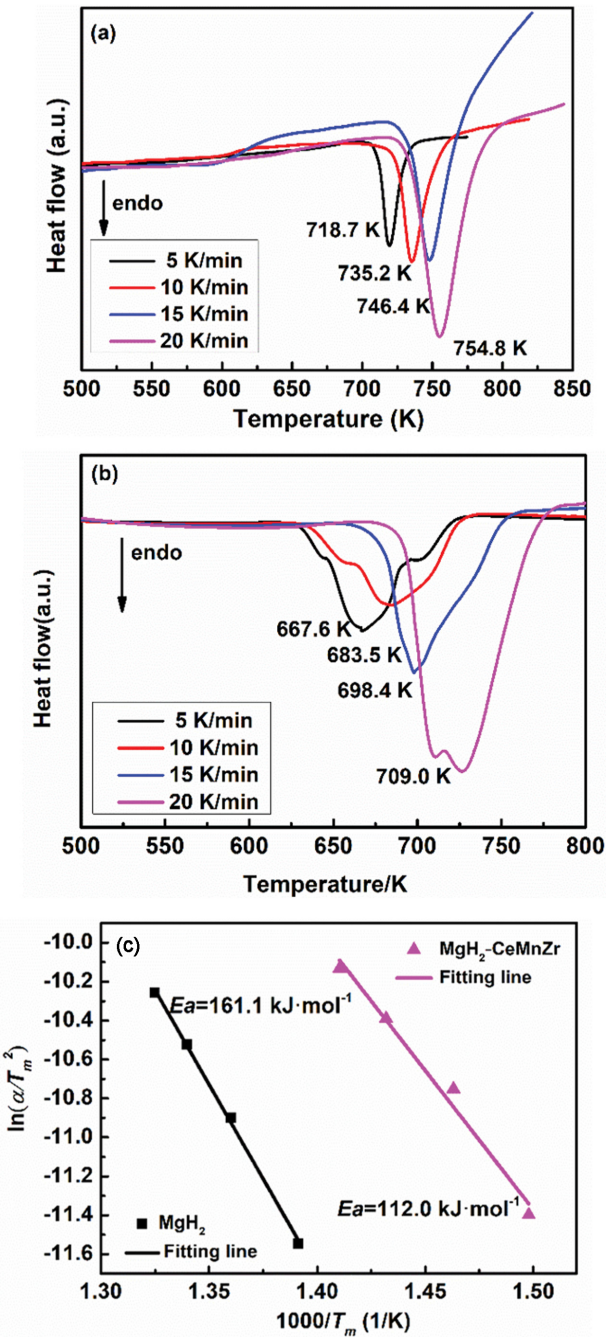

Fig. 4. DSC curves of MgH_2 (a) and MgH_2-CeMnZr composite (b) at different heating rates 5 K/min, 10 K/min, 15 K/min, 20 K/min; (c) The Kissinger plot of decomposition for CeMnZr-doped MgH_2 composite and milled MgH_2.

follows:

$$\frac{d[\ln(\alpha/T_m^2)]}{d(1/T_m)} = \frac{-E_a}{R} \quad (1)$$

where α is the different rise rate (K/min), T_m is the peak temperature (K) for the different heating rate in Fig. 4, and R is the gas constant (8.314 $J \cdot mol^{-1} \cdot K^{-1}$). Fig. 4 presents the DSC curves at different heating rate for the as-milled MgH_2 and CeMnZr catalyzed MgH_2 composites. Note that the E_a value for the hydrogen desorption is estimated to be 161.1 $kJ \cdot mol^{-1}$ for the milled MgH_2, where the value for CeMnZr doped sample is reduced to 112.0 $kJ \cdot mol^{-1}$, which is about 50 kJ mol^{-1} lower than the value of the milled MgH_2. The value of E_a achieved by the Kissinger analysis proves that the addition of CeMnZr can decrease the dehydrogenation reaction energy barrier of the doped sample, which obviously promotes the desorption property of MgH_2.

To verify the catalytic influence of the doped CeMnZr on the hydrogen absorption of pristine MgH_2, the hydrogen sorption properties of the as-milled MgH_2 and CeMnZr-doped MgH_2 at 423 K and 473 K were tested after completely finishing the hydrogen dehydrogenation process. The hydrogen absorption curves of the as-milled MgH_2 and CeMnZr-doped MgH_2 at 423 K and 473 K are presented in Fig. 5. It is obvious that almost no hydrogen can be absorbed by as-milled MgH_2 at 423 K within 3,500 s. The hydrogen absorption behavior shows an upward trend when the temperature increases to 473 K, which is corresponding to previous studies that the increased temperature is beneficial to the improved hydrogen absorption ability [32]. At 473 K, the as-milled MgH_2 can uptake 1.83 wt% hydrogen in 3,500 s under the hydrogen pressure of 3.0 MPa. With the introduction of CeMnZr catalyst, the MgH_2-CeMnZr sample exhibits better hydrogen absorption ability than the as-milled MgH_2. At 423 K, 3.32 wt% of hydrogen can be uptaken rapidly by the MgH_2-CeMnZr sample, where the as-milled MgH_2 requires a higher temperature to achieve the same amount of the hydrogen sorption as MgH_2-CeMnZr sample. At 473 K, the MgH_2-CeMnZr sample has the hydrogen absorption capacity of about 4.08 wt% within 3,500 s, which is more than twice higher the as-milled MgH_2. As compared to the mentioned results comprehensively, it is confirmed that the addition of CeMnZr solid solution catalyst has promoted the hydrogen storage properties of MgH_2 effectively.

To understand how the doped CeMnZr solid solution affects the hydrogen sorption kinetics of MgH_2, the hydrogen absorption mechanism is discussed by fitting the hydrogen absorption curves for the doped and undoped samples through the Johnson-Mehl-Avrami (JMA) model and Arrhenius analysis by fitting the absorption curves of MgH_2. The well-known JMA model is conducive to understanding the hydrogenation absorption process and enhancing the comprehension for the reaction mechanism. The equation used in JMA model is as follows:

$$kt = [-\ln(1-\alpha)]^{1/n} \quad (2)$$

In which α and k represent the reacted fraction, rate constant, respectively. The Avrami exponent n is generally used to understand the dimensionality of the growth process and the information about the rate-limiting step of the reaction. Clearly, as seen from Fig. 5, when α(t) varies from 0.2 to 0.8 the ln[ln(1−α(t))] shows a straight line against ln(t). Therefore, the JMA equation is well suited to investigate the hydrogenation mechanism of pure MgH_2 and MgH_2-CeMnZr composites. Interestingly, the Avrami exponent n is 0.33 at 473 K and 0.39 at 523 K for the MgH_2-CeMnZr composites, continuously shifts to 0.45 at 573 K. In the hydrogenation process, the Avrami exponent n at different temperature is close to 0.5, indicating that the hydrogenation of the MgH_2-CeMnZr nano-

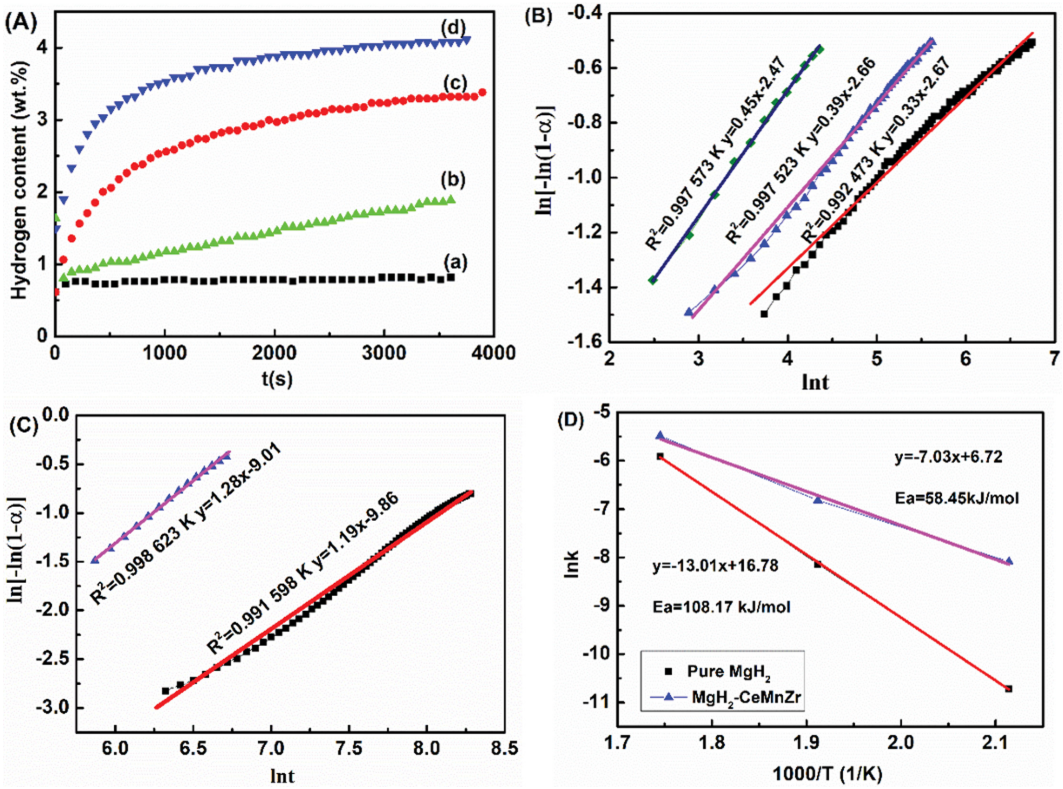

Fig. 5. (A) The hydrogen absorption curves of the sample at different temperature under 3.0 MPa: (a) as-milled MgH_2 at 423 K; (b) as-milled MgH_2 at 473 K; (c) CeMnZr-doped MgH_2 composite at 423 K; (d) CeMnZr-doped MgH_2 composite at 473 K; JMA plots for the isothermal reaction of MgH_2-CeMnZr: (B) rehydrogenation and (C) dehydrogenation; (D)Arrhenius plots for the rehydrogenation of MgH_2-CeMnZr and MgH_2.

composite is mainly controlled by the hydrogen diffusion. The hydrogen desorption data at 598 and 623 K are fitted with JMA model and shown in Fig. 5(c). It is observed that the linear relationship is fitted very well. The Avrami exponent n value of dehydrogenation for different temperatures is ~1, whose rate limiting step lies in one-dimensional growth with constant interface velocity. This value range indicates that the hydrogen absorption and desorption process of MgH_2-CeMnZr composite is mainly controlled by hydrogen diffusion and one-dimensional growth with constant interface velocity, respectively. Furthermore, the calculated activation energy (E_a) values for these composites are shown in typical Arrhenius plots in Fig. 5(d). As expected, the calculated E_a value for the hydrogen absorption process is 58.45 kJ mol^{-1} for MgH_2-CeMnZr composite, much lower than 108.17 kJ mol^{-1} for MgH_2, giving further evidence for the relevance between the addition of CeMnZr and the hydrogen absorption kinetics. The dopant of CeMnZr into MgH_2 can effectively reduce the kinetic energy barrier of hydrogen absorption reaction of Mg based hydrogen storage materials and thus improve their kinetic properties.

3. Catalytic Mechanism

To clearly clarify the phase transformation between MgH_2 and CeMnZr solid solution at different stage, XRD was employed to analyze the phase constitution of the MgH_2-CeMnZr composite. Fig. 6 exhibits the XRD patterns of the ball-milled, hydrogenation, dehydrogenation process. As illuminated in Fig. 6(a), the dominant

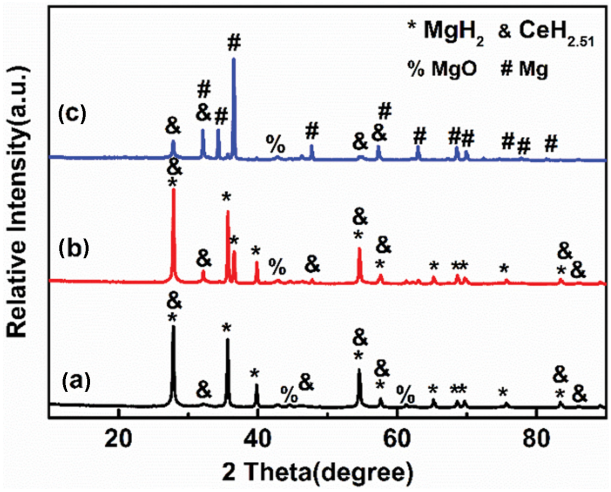

Fig. 6. XRD profiles of (a) as-milled, (b) hydrogenation and (c) dehydrogenation of the MgH_2-CeMnZr composite.

diffraction peak is ascribed to MgH_2. Additionally, new peaks that are composed of MgO and $CeH_{2.51}$ are found with the disappearance of CeMnZr solution solid catalyst; the presence of MgO may be due to the little oxidation generated from the sample operation processing, while the new diffraction peaks of $CeH_{2.51}$ are detected

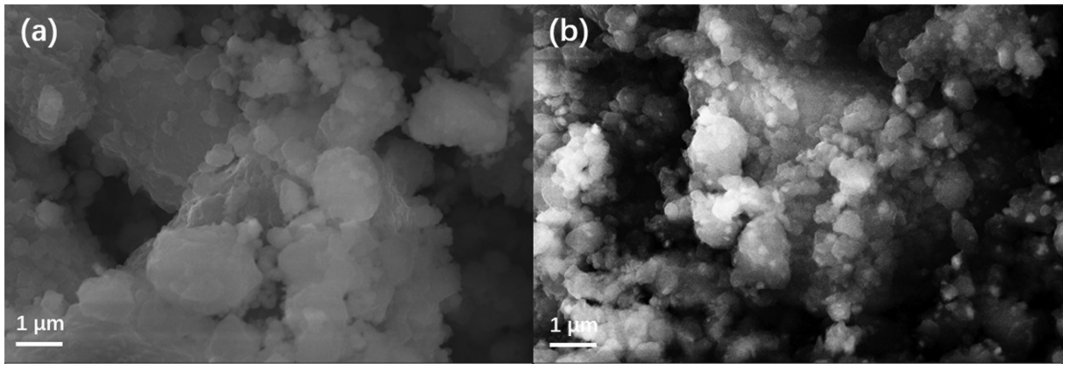

Fig. 7. SEM images for the as-milled MgH_2 (a) and CeMnZr doped MgH_2 sample (b).

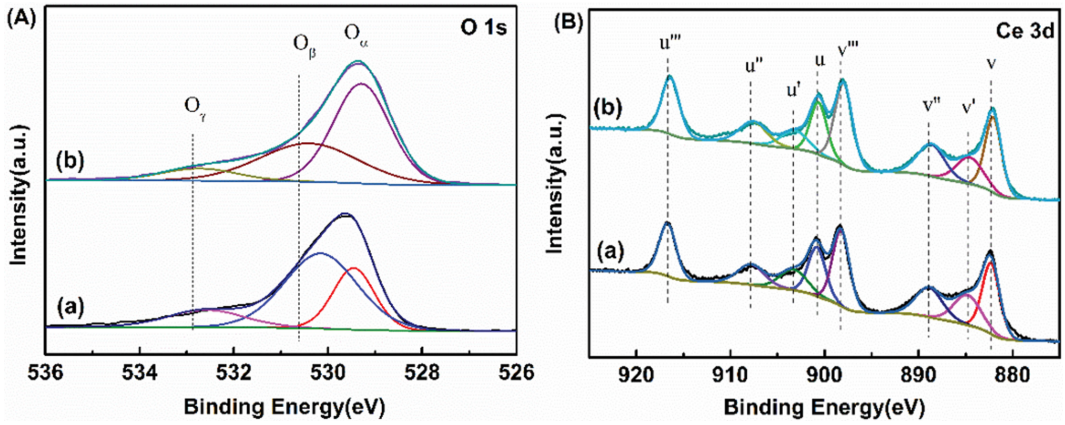

Fig. 8. XPS curves of O 1s (A) and Ce 3d (B) for the samples (a) pure CeO_2 (b) CeMnZr solid solution.

in the MgH_2-CeMnZr composite, substantiating that there an obvious chemical reaction occurred between MgH_2 and CeMnZr solid solution in the ball milling process. After hydrogenation at 3.0 MPa, it can be found that the MgH_2, MgO and $CeH_{2.51}$ phases are still clearly visible in the hydrogenation state. For the dehydrogenated at 0.1 MPa, as shown in Fig. 6(c), the diffraction peaks of Mg appear accompanied by the disappearance of the MgH_2 peaks. The peaks of $CeH_{2.51}$ and MgO phase could be still clearly seen in the dehydrogenation process. Note that Mn and Zr could not be detected in the whole XRD patterns, which is due to the formation of solid solution; moreover, the obtained results are in accord with the XRD analysis in Fig. 1. Referring to the XRD analysis, the diffraction peaks for $CeH_{2.51}$ and MgO still exist in the whole hydrogenation/dehydrogenation process; $CeH_{2.51}$ and MgO may be the favorable phase for the enhancement of hydrogen storage for the as-milled MgH_2. Nevertheless, numerous researches have proved that the newly appeared $CeH_{2.51}$ is in favor for the improvement of the MgH_2 hydrogen absorption/desorption [32].

To further investigate the doped CeMnZr on the effect of the morphology for the pristine MgH_2, SEM analysis was used and the corresponding image is shown in Fig. 7. Obviously, the as-milled MgH_2 presents irregular shape with a wide size range. It can be seen that the CeMnZr added sample exhibits a smaller grain size with loose structure than the as-milled MgH_2, indicating that the addition of CeMnZr solid solution is helpful for the particle reduction of MgH_2 to prevent the formation of large clusters. The decreased particle size promotes the performance of hydrogen absorption and desorption for Mg and Mg-based materials. Therefore, the addition of CeMnZr solid solution significantly decreases the particle size of MgH_2 and is conducive to altering the hydrogen absorption/desorption properties.

To further clarity the mechanism for the doped CeMnZr which catalyzes the improvement of hydrogen sorption performance for MgH_2, the composition of surface elements and adsorbed oxygen species for the pure CeO_2 and CeMnZr was characterized by XPS. Fig. 8 displays the XPS spectra of Ce 3d, O 1s for the pure CeO_2 and CeMnZr solid solution. With regard to Fig. 8(a), there exist three dominant fitting peaks: The peak located at 529.4 eV (O_α) is attributed to the lattice oxygen (O^{2-}), while the peaks centered at O_β (530.6 eV) and O_γ (532.9 eV) are assigned to chemically adsorbed oxygen (O^-, O_2^-), respectively. Zhou et al. [21,22] reported that the surface lattice oxygen as the active oxygen species is beneficial to improving the hydrogen sorption behavior, owing to its abundant oxygen vacancy. It can be seen from Fig. 8(a) more lattice oxygen O_α on the surface of CeMnZr solid solution than the pure CeO_2, giving an indication that more oxygen vacancies exist in the Mn and Zr doped CeO_2.

With regard to Fig. 8(b), Ce 3d is numerically decomposed into eight components for each sample, and the corresponding assignments are labeled as V (882.3 eV), V′ (884.6 eV), V″ (888.8 eV), V‴

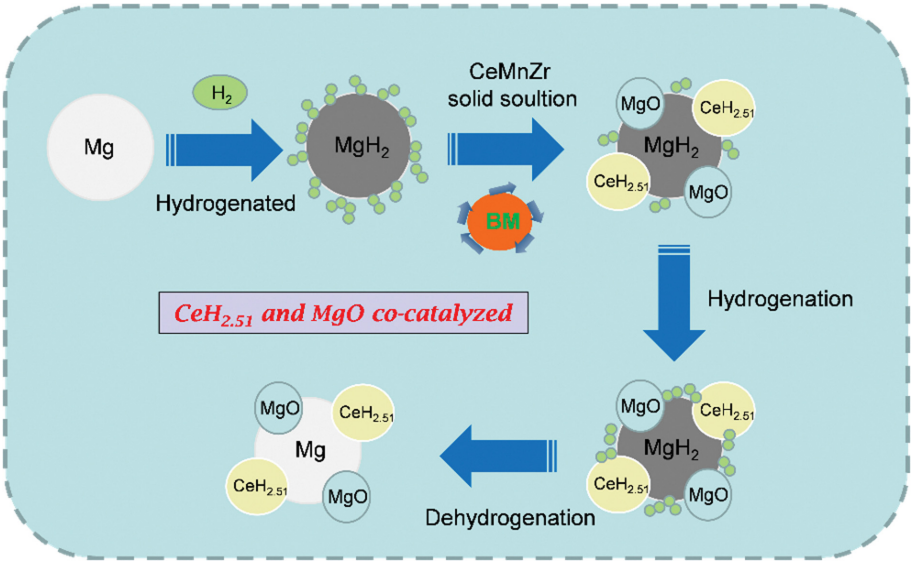

Fig. 9. The mechanism diagram for the CeMnZr doped MgH_2.

(898.3 eV), U (900.8 eV), U′ (903.3 eV), U″ (907.9 eV), U‴ (916.7 eV). The fitting peaks centered at V, V″, V‴, U, U″, U‴ are related to the Ce^{4+} species, and the other peaks labeled V′ and U′ represent the Ce^{3+} species, which is the central chemical valance state on the surface of the sample. In Fig. 8(b), the amount of Ce^{3+} on the surface of CeMnZr is higher than the pure CeO_2. As confirmed by Huang [33] and Weng [34] et al., the pronounced catalytic activity was caused by the formation of more Ce^{3+} accompanied with oxygen defects. On the basis of the obtained XPS analysis, the Mn and Zr doped CeO_2 has more oxygen vacancies and Ce^{3+} on the CeMnZr surface.

Referring to the mentioned analysis, the improvement in the hydrogen sorption kinetics of MgH_2-CeMnZr composites is speculated to those reasons and the corresponding mechanism diagram is described in Fig. 9: (1) the $CeH_{2.51}$ compound formed during the ball-milling process has promoted the improvement of hydrogen sorption performance for MgH_2. As reported by zheng et al. [35], $CeH_{2.51}$ had a better catalytic effect on hydrogen sorption kinetics of solid state hydrogen storage material, which happened because $CeH_{2.51}$ mainly exerted its influence on the contact surface. Ismail et al. also discovered that cerium hydride was a cracking agent that introduced an extra catalytic effect on metal hydride sorption properties [36]. (2) Other than $CeH_{2.51}$, the formation of MgO was substantiated to make a contribution to the striking hydrogen storage behavior for Mg-based materials. A study made by Aguey-Zinsou et al. that the magnesium that milled with MgO exhibited excellent hydring and dehydring kinetics, the absorption or desorption of hydrogen takes place in less than 150 s with a capacity of 6.5 wt% hydrogen [37]. Ares-Fernández demonstrated that the kinetics of hydrogen absorption/desorption in magnesium catalyzed by MgO was found to be more effective than the best catalyst Nb_2O_5 [38]. (3) Additionally, the abundant oxygen vacancies and the reduced particle size due to the Mn and Zr doped also play a vital role for the enhancement of the hydrogen sorption kinetics [21,22]. Hence, the mechanism of MgH_2 catalyzed by CeMnZr is mainly ascribed to the in-situ formation of $CeH_{2.51}$, MgO as well as the abundant oxygen vacancies and the reduced particle size, CeMnZr is proved to be the prominent catalyst in boosting the hydrogen storage properties of MgH_2.

CONCLUSIONS

The solid solution CeMnZr was synthesized and its catalytic effect on the hydrogen sorption properties of MgH_2 was systemically investigated. The introduced CeMnZr catalyst effectively improved the hydrogen absorption/desorption kinetics and lowered the desorption temperature of the pristine MgH_2. The MgH_2-CeMnZr sample could absorb 3.32 wt% of hydrogen at 423 K and 4.08 wt% of hydrogen could be obtained at 473 K within 3,500 s, whereas the pristine MgH_2 almost showed no hydrogen ability at 423 K and only 1.83 wt% of hydrogen could be taken up in 3,500 s at 473 K. Moreover, the desorption capacity and rate are highly enhanced for the composite which had a desorption capacity of 2.56 wt% at 573 K and 4.84 wt% at 623 K. From the Kissinger analysis calculation, the apparent dehydrogenation activation energy for the MgH_2-CeMnZr sample was 112.0 $kJ \cdot mol^{-1}$, which is about 50 $kJ \cdot mol^{-1}$ lower than the as-milled MgH_2. From these results, it can be concluded that the in-situ generated MgO and $CeH_{2.51}$ species as well as the abundant oxygen vacancy is believed to have synergistic catalytic effects in enhancing the hydrogen storage properties of the CeMnZr coped MgH_2 composite.

ACKNOWLEDGEMENTS

This work was supported by Natural Science Foundation of Hebei Province of China (E2019415036); Science and Technology Project of Hebei Education Department (BJ2020043); Hebei University of Environmental Engineering (Top-notch Talents Cultivation Program for Young Science and Technology 2020ZRBJ01); Doctoral Foundation of Hebei University of Environmental Engi-

neering (201805).

DECLARATIONS

Conflict of Interest

The authors declare that they have no known competing financial interests or personal relationships that could have appeared to influence the work reported in this paper.

Ethics Approval

This study does not contain experiments that involve humans or animals other than the authors who performed the work.

Informed Consent

Not applicable.

REFERENCES

1. X. Zhang, Y. Liu, Z. Ren, X. Zhang, J. Hu, Z. Huang, Y. Lu, M. Gao and H. Pan, *Energ. Environ. Sci.*, **14**, 2302 (2021).
2. K. Hyun, S. Kang and Y. Kwon, *Korean J. Chem. Eng.*, **36**, 500 (2019).
3. S. Kim, J. Song and H. Lim, *Korean J. Chem. Eng.*, **35**, 1509 (2018).
4. D. J. Han, K. R. Bang, H. Cho and E. S. Cho, *Korean J. Chem. Eng.*, **37**, 1306 (2020).
5. W. Zhang, Y. Cheng, Y. Li, Z. Duan and J. Liu, *J. Rare Earth*, **33**, 334 (2015).
6. N. A. Abdul Majid, J. Watanabe and M. Notomi, *Int. J. Hydrogen Energy*, **46**, 4181 (2021).
7. Y. Fang, J. Zhang, M. Y. Hua and D. W. Zhou, *J. Mater. Sci.*, **55**, 1959 (2020).
8. N. Roy, S. Kumari, Harshit, P. P. Jana and P. A. Deshpande, *J. Solid State Chem.*, **304**, 122560 (2021).
9. N. Khossossi, Y. Benhouria, S. R. Naqvi, P. K. Panda, I. Essaoudi, A. Ainane and R. Ahuja, *Sustain. Energ. Fuels*, **4**, 4538 (2020).
10. M. D. Seo, A. Kim and H. Jung, *J. Solid State Chem.*, **269**, 151 (2019).
11. T. Huang, X. Huang, C. Hu, J. Wang, H. Liu, Z. Ma, J. Zou and W. Ding, *Mater Today Energy*, **19**, 100613 (2021).
12. W. Zhu, S. Panda, C. Lu, Z. Ma, D. Khan, J. Dong, F. Sun, H. Xu, Q. Zhang and J. Zou, *ACS Appl. Mater. Inter.*, **12**, 50333 (2020).
13. Y. Zhao, Y. Zhu, J. Liu, Z. Ma, J. Zhang, Y. Liu, Y. Li and L. Li, *J. Alloys Compd.*, **862**, 158004 (2021).
14. H. Cao, C. Pistidda, M. V. Castro Riglos, A.-L. Chaudhary, G. Capurso, J.-C. Tseng, J. Puszkiel, M. T. Wharmby, T. Gemming, P. Chen, T. Klassen and M. Dornheim, *Sustain. Energ. Fuels*, **4**, 1915 (2020).
15. M. Ismail, *Int. J. Hydrogen Energy*, **46**, 8621 (2021).
16. D. J. Han, S. Kim and E. S. Cho, *J. Mater. Chem. A*, **9**, 9875 (2021).
17. S. Gao, X. Wang, H. Liu, T. He, Y. Wang, S. Li and M. Yan, *J. Power Sources*, **438**, 227006 (2019).
18. L. S. Xie, J. S. Li, T. B. Zhang and L. Song, *Mater. Charact.*, **133**, 94 (2017).
19. R. K. Singh, T. Sadhasivam, G. I. Sheeja, P. Singh and O. N. Srivastava, *Int. J. Hydrogen Energy*, **38**, 6221 (2013).
20. X. Zhu, L. Sun, Y. Zheng, H. Wang, Y. Wei and K. Li, *Int. J. Hydrogen Energy*, **39**, 13381 (2014).
21. P. Liu, H. Chen, H. Yu, X. Liu, R. Jiang, X. Li and S. Zhou, *Int. J. Hydrogen Energy*, **44**, 13606 (2019).
22. P. Liu, J. J. Lian, H. P. Chen, X. J. Liu, Y. L. Chen, T. H. Zhang, H. Yu, G. J. Lu and S. X. Zhou, *Chem. Eng. J.*, **385**, 123448 (2020).
23. J. Yu, Z. Si, L. Chen, X. Wu and D. Weng, *Appl. Catal. B*, **163**, 223 (2015).
24. D. Shang, Q. Zhong and W. Cai, *J. Mol. Catal. A: Chem.*, **399**, 18 (2015).
25. M. P. Yeste, M. Á. Cauqui, J. Giménez-Mañogil, J. C. Martínez-Munuera, M. Á. Muñoz and A. García-García, *Chem. Eng. J.*, **380**, 122370 (2020).
26. S. Ali, L. Chen, F. Yuan, R. Li, T. Zhang, S. u. H. Bakhtiar, X. Leng, X. Niu and Y. Zhu, *Appl. Catal. B*, **210**, 223 (2017).
27. P. Meena, M. Jangir, A. Kumar, R. Singh, V. K. Sharma and I. P. Jain, *Mater. Res. Express*, **4**, 116520 (2017).
28. N. H. Idris, N. S. Mustafa and M. Ismail, *Int. J. Hydrogen Energy*, **42**, 21114 (2017).
29. L. Wei, H. Gu, Y. Zhu and L. Li, *Int. J. Hydrogen Energy*, **37**, 17146 (2012).
30. H. J. Zhu, Y. Y. Chen, Y. B. Gao, W. X. Liu, Z. P. Wang, C. C. Cui, W. Liu and L. G. Wang, *J. Rare Earth*, **37**, 961 (2019).
31. T. Yao, Y. Uckimoto, T. Sugiyama and Y. Nagai, *Solid State Ionics*, **35**, 359 (2000).
32. N. S. Mustafa and M. Ismail, *J. Alloys Compd.*, **695**, 2532 (2017).
33. X. Yuan, H. Ge, X. Liu, X. Wang, W. Chen, W. Dong and F. Huang, *J. Alloys Compd.*, **688**, 613 (2016).
34. J. Fan, X. Wu, X. Wu, Q. Liang, R. Ran and D. Weng, *Appl. Catal. B: Environ.*, **81**, 38 (2008).
35. H.-Y. Zheng, Z.-Q. Ding, Y.-J. Xie, J.-F. Li, C.-K. Huang, W.-T. Cai, H.-Z. Liu and J. Guo, *Int. J. Hydrogen Energy*, **46**, 4168 (2021).
36. M. Ismail, N. S. Mustafa, N. Juahir and F. A. H. Yap, *Mater. Chem. Phys.*, **170**, 77 (2016).
37. K. F. Aguey-Zinsou, J. R. Ares Fernandez, T. Klassen and R. Bormann, *Mater. Res. Bull.*, **41**, 1118 (2006).
38. J.-R. Ares-Fernández and K.-F. Aguey-Zinsou, *Catalysts*, **2**, 330 (2012).